Journal of Solid State Chemistry 183 (2010) 2032–2039

Contents lists available at ScienceDirect

Journal of Solid State Chemistry

journal homepage: www.elsevier.com/locate/jssc

Syntheses and crystal structures of RE_3MnSn_{5-x} (RE=Tm, Lu) with 3D Mn–Sn framework

Xiao-Wu Lei [a,b], Chun-Li Hu [a], Jiang-Gao Mao [a,*]

[a] State Key Laboratory of Structural Chemistry, Fujian Institute of Research on the Structure of Matter, Chinese Academy of Sciences, Fuzhou 350002, PR China
[b] Graduate School of the Chinese Academy of Sciences, Beijing 100039, PR China

ARTICLE INFO

Article history:
Received 25 March 2010
Received in revised form
24 June 2010
Accepted 3 July 2010
Available online 23 July 2010

Keywords:
Intermetallics
Crystal structures
Stannides
Electronic structure calculation

ABSTRACT

Four new isostructural rare earth manganese stannides, namely RE_3MnSn_{5-x} (x=0.16(6), 0.29(1) for RE=Tm, x=0.05(8), 0.21(3) for RE=Lu), have been obtained by reacting the mixture of corresponding pure elements at high temperature. Single-crystal X-ray diffraction studies revealed that they crystallized in the orthorhombic space group *Pnma* (No. 62) with cell parameters of a=18.384(9)–18.495(6) Å, b=6.003(3)–6.062(2) Å, c=14.898(8)–14.976(4) Å, V=1644.3(14)–1679.0(9) Å^3 and Z=8. Their structures belong to the $Hf_3Cr_2Si_4$ type and feature a 3D framework composed of 1D $[Mn_2Sn_7]$ chains interconnected by $[Sn_3]$ double chains via Sn–Sn bonds, forming 1D large channels based on $[Mn_4Sn_{16}]$ 20-membered rings along the b-axis, which are occupied by the rare earth atoms. Electronic structure calculations based on density functional theory (DFT) for idealized "RE_3MnSn_5" model indicate that these compounds are metallic, which are in accordance with the results from temperature-dependent resistivity measurements.

1. Introduction

Ternary rare-earth (RE) transition-metal (TM) tetrelides *RE*–TM–*Tt* (*Tt*=Si, Ge, Sn) have been extensively investigated in the past several decades due to their remarkable structural diversity and novel chemical bonding [1–11]. These compounds display interesting physical properties associated with either RE or/and TM substructure. For example, some ternary tetrelides of $Yb_3Rh_4Sn_{13}$ or $Sc_5Co_4Si_{10}$ type structure display coexistence of superconductivities and magnetic properties [12,13]; cerium stannides exhibit a variety of unusual physical properties such as long-range magnetic ordering, Kondo effect, and coexistence of heavy fermion behavior and superconductivity or valence fluctuation behavior [14,15].

Among these phases, those containing a late transition metal (such as Co, Ni, Cu, Zn) are now relatively well known [16–26]; however, reports on those containing manganese metal are still scarce. It is reported that manganese-based tetrelides also display interesting structural characters. For example, the equiatomic *RE*Mn*Tt* (*Tt*=Si, Ge) of CeFeSi-type feature a 2D corrugated [Mn*Tt*] layer separated by rare earth atoms [27,28], and *RE*Mn_2Tt_2 (*Tt*=Si, Ge) of $ThCr_2Si_2$-type feature a 3D framework composed of the same 2D [Mn*Tt*] layers interconnected via direct *Tt*–*Tt* bonds [29–31]. Similarly, the structure of *RE*$MnSi_2$ ($CeNiSi_2$-type) features a 3D framework composed of the same 2D [MnSi] layers and zigzag Si chains interconnected via Si–Si bonds [32–34]. With a higher tetrel metal content, a series of $HfFe_6Ge_6$-type compounds, *RE*Mn_6Tt_6 (*Tt*=Ge, Sn), have attracted considerable interest in recent years due to out-standing magnetoresistance properties and potential applications in magnetic storage devices [35–37]. It should be noted that the Mn element is apt to form various magnetic substructure based on strong Mn–Mn interaction. For example, there exists 2D square-net layer with short Mn–Mn distances of 2.8–3.0 Å in the structures of *RE*MnTt, *RE*Mn_2Tt_2 and *RE*$MnSi_2$, whereas it forms 2D hexagonal-net layer with short Mn–Mn distances of 2.6–2.8 Å in the REMn_6Tt_6 (*Tt*=Ge, Sn) phases. In addition, $Tb_3Mn_4Ge_4$ ($Zr_3Cu_4Si_4$-type), $Tm_4Mn_4Sn_7$ ($Zr_4Co_4Ge_7$-type) and $RE_2Mn_3Si_5$ (*RE*=Tb–Tm, $Sc_2Fe_3Si_5$-type) have also been reported with abundant magnetic properties [38–40].

Intrigued by the rich structural types and novel physical properties of these manganese-based tetrelides, we undertook systematic studies in the ternary *RE*–Mn–Sn system, about which much less is known compared with the corresponding silicides and germanides. Our exploratory studies afforded the ternary $Yb_4Mn_2Sn_5$ (Mg_5Si_6-type) [20], and attempts to prepare other rare earth analogs led to a series of new ternary stannides, namely RE_3MnSn_{5-x} (x=0.16(6), 0.29(1) for RE=Tm, x=0.05(8), 0.21(3) for RE=Lu). Their structures belong to the $Hf_3Cr_2Si_4$ type [41] and feature a 3D framework composed of 1D $[Mn_2Sn_7]$ chains interconnected by $[Sn_3]$ double chains via Sn–Sn bonds, forming 1D large tunnels along the b-axis occupied by rare earth atoms.

* Corresponding author. Fax: +86 591 83704836.
E-mail address: mjg@fjirsm.ac.cn (J.-G. Mao).

0022-4596/$ - see front matter © 2010 Elsevier Inc. All rights reserved.
doi:10.1016/j.jssc.2010.07.003

Herein, we report their syntheses, crystal structures, band structures and physical properties.

2. Experimental section

2.1. Preparation of RE_3MnSn_{5-x} (RE=Tm, Lu)

All manipulations were performed inside an argon-filled glove box with moisture level below 1 ppm. All starting materials were used as received: rare earth blocks (Acros, 99.99%), manganese powder (Shanghai fourth chemical reagent company, 99.99%) and tin granules (Acros, 99.99%). It should be noted that the purity of manganese powder corresponds to the metals purity and its surface may contain small amount of metal oxide impurity due to the oxide formation on the surface. Single crystal of Tm_3MnSn_{5-x} (x=0.29(1)) was initially obtained by reacting the mixture of Tm, Mn and Sn metal in molar ratio of 4:2:5 during our attempts to prepare the Tm analog of $Yb_4Mn_2Sn_5$. The sample was loaded into a niobium tube, which was subsequently arc-welded under argon atmosphere and sealed in the quartz tube under vacuum ($\sim 10^{-4}$ Torr). The quartz tube was put into a high-temperature furnace and allowed to react at 980 °C for 7 days, and then it was allowed to cool at a rate of 0.1 °C/min to room temperature. The prism-shaped crystal of Tm_3MnSn_{5-x} (x=0.29(1)) was selected for structure determination. Attempts to prepare other analogies led to isostructural compounds of Tm_3MnSn_{5-x} (x=0.16(6)) and Lu_3MnSn_{5-x} (x=0.05(8), 0.21(3)). After proper structural analyses, these compounds were prepared in a high yield and high purity by the reaction of the mixture of the pure metals in tantalum tubes according to the loading composition of "RE_3MnSn_5". The use of Ta tubes instead of Nb tubes was to eliminate binary Nb_3Sn impurity found in the products when Nb tubes were used. The samples were reacted at 1050 °C for 7 days and annealed at 650 °C for 15 days, and then they were allowed to slowly cool to room temperature. The purities of the sample were confirmed by the X-ray powder diffraction studies (see Supplementary materials).

2.2. Elemental analysis

Semi-quantitative microprobe elemental analyses for *RE*, Mn and Sn were performed on a JSM-6700F scanning electron microscope (SEM) equipped with an energy dispersive spectroscope (EDS) detector. Data were acquired with an accelerating voltage of 20 KV and SEM of 40°. Visibly clean surfaces of crystals were selected for analysis and high magnifications were used during data collection in order to obtain accurate results. The microprobe elemental analyses on single crystals of Tm_3MnSn_{5-x} (x=0.29(1)) and Lu_3MnSn_{5-x} (x=0.21(3)) indicated the presence of *RE*, Mn and Sn elements in molar ratios of 3.0(8):1.2(7):4.9(6) and 3.0(7):1.3(6):5.1(6), respectively, which are in agreement with the results derived from the single crystal X-ray diffraction refinements.

2.3. Crystal structure determination

Single crystals of the title compounds were selected from the reaction products and sealed into thin-walled glass capillaries within the glove-box. Data collections for the four compounds were performed on a Rigaku Mercury CCD (Mo$K\alpha$ radiation, graphite monochromator) at 293(2) K. All the data sets were corrected for Lorentz factor, polarization, air absorption and absorption due to variations in the path length through the detector faceplate. Absorption corrections based on the multi-scan method were also applied [42].

All the structures were solved using direct methods (SHELX-97), and refined by least-square methods with atomic coordinates and anisotropic thermal parameters [43]. The space group for RE_3MnSn_{5-x} (*RE*=Tm, Lu) was determined to be *Pnma* (No. 62) based on systematic absences, *E* value statistics and satisfactory refinements. Site occupancy refinements indicated that all sites were fully occupied except Sn(5) sites in the four compounds as well as Sn(7) sites in the compounds **1**, **2** and **4**. The occupancy factors of Sn(5) sites were refined to be 81.3(7)%, 76.7(1)%, 89.5(3)% and 81.3(4)%, respectively, for compounds **1**–**4**, and those of Sn(7) sites were refined to be 92.9(1)%, 82.6(4)% and 88.5(5)% for compounds **1**, **2** and **4**, respectively. Final difference Fourier maps showed featureless residual peaks of 2.24 e/Å^3 (2.07 Å from Sn(6) atom) and −2.83 e/Å^3 (0.70 Å from Sn(5) atom) for **1**, 2.95 e/Å^3 (0.92 Å from Tm(3) atom) and −2.21 e/Å^3 (0.79 Å from Sn(5) atom) for **2**, 2.11 e/Å^3 (0.73 Å from Sn(5) atom) and −1.77 e/Å^3 (0.73 Å from Sn(5) atom) for **3**, 2.72 e/Å^3 (1.17 Å from Sn(3) atom) and −3.42 e/Å^3 (0.95 Å from Lu(2) atom) for **4**. The details of the crystallographic data and refinement parameters for the four compounds are summarized in Table 1. Atomic coordinates and important bond distances are listed in Tables 2–4.

Crystallographic data in CIF format for RE_3MnSn_{5-x} (x=0.16(6), 0.29(1) for *RE*=Tm, x=0.05(8), 0.21(3) for *RE*=Lu) have been given as Supplementary materials. These data can also be obtained from the Fachinformationszentrum Karlsruhe, 76344 Eggenstein-Leopoldshafen, Germany (fax: +49 7247 808 666; e-mail: crysdata@fiz-karlsruhe.de) on quoting the depository numbers CSD of 421559, 421560, 421561 and 421562.

2.4. Property measurements

The polycrystalline samples were grinded to fine powders, which was uniform in color and morphology and contained no other detectable phases as judged by its X-ray diffraction pattern. The X-ray diffraction (XRD) powder patterns were collected at room temperature on a X'Pert-Pro diffractometer using Cu$K\alpha$ radiation (λ=1.5406 Å) in the 2θ range of 5–85° with a step size of 0.04° and 10 s/step counting time. The samples were cold-pressed into $5.0 \times 3.0 \times 7.0$ mm^3 bar-shaped pellets whose density attain ~80% of the theoretical values calculated from the formula refined from the single-crystal X-ray data. The resistivity measurements were performed on a Quantum Design PPMS-9 magnetometer using a standard four-probe technique in the temperature range of 5–300 K. The measurements were carried out while gradually warming the sample that was initially cooled to 5 K at zero field.

2.5. Electronic structure calculations

To better understand the electronic structures of the title compounds, ab initio electronic structure calculations were carried out for idealized "RE_3MnSn_5" model, where all the Sn sites were assumed to be fully occupied. The calculations were performed with full-potential linearized augmented plane wave plus local basis (FPLAPW+lo) method based on the density functional theory (DFT), using the general gradient approximation (GGA-PBE) to treat the exchange and correlation potential, as implemented in the WIEN2K package [44–47]. Within the FPLAPW method, the space was divided into nonoverlapping muffin-tin (MT) spheres and interstitial region. The parameter $R_{MT} \times K_{MAX}$ (R_{MT} is the smallest muffin-tin spherical radius present in the system and K_{MAX} is the maximum modulus for

Table 1
Single crystal data and structure refinements for Tm_3MnSn_{5-x} with $x=0.16(6)$ (**1**), 0.29(1) (**2**) and Lu_3MnSn_{5-x} with $x=0.05(8)$ (**3**) and 0.21(3) (**4**).

Compounds	**1**	**2**	**3**	**4**
Chemical formula	$Tm_3MnSn_{4.84}$	$Tm_3MnSn_{4.71}$	$Lu_3MnSn_{4.95}$	$Lu_3MnSn_{4.79}$
fw	1135.71	1120.76	1167.13	1148.73
Space group	*Pnma* (No. 62)	*Pnma* (No. 62)	*Pnma* (No. 62)	*Pnma* (No. 62)
a/Å	18.495(6)	18.449 (1)	18.417(4)	18.384(9)
b/Å	6.062(2)	6.0128(4)	6.045(1)	6.003(3)
c/Å	14.976(4)	14.9328(8)	14.939(3)	14.898(8)
V(Å^3)	1679.0(9)	1656.5 (2)	1663.3(6)	1644.3(1)
Z	8	8	8	8
D_{calcd} (g cm^{-3})	8.986	8.988	9.322	9.281
Temp (K)	293(2)	293(2)	293(2)	293(2)
μ (mm^{-1})	46.822	47.085	51.201	51.332
Crystal size (mm)	$0.18\times0.04\times0.04$	$0.22\times0.06\times0.05$	$0.15\times0.03\times0.03$	$0.20\times0.05\times0.05$
Index ranges	$(-23, 24), \pm7, \pm19$	$\pm23, \pm7, (-16, 19)$	$(-23, 19), \pm7, \pm19$	$(-23, 21), \pm7, \pm19$
Reflections collected	12686	12462	12523	12644
Unique reflections	2099	2069	2054	2058
Reflections ($I>2\sigma(I)$)	1927	1972	1784	1838
GOF on F^2	1.173	1.162	1.125	1.148
$R1$, w$R2(I>2\sigma(I))$[a]	0.0292/0.0526	0.0255/0.0539	0.0187/0.0422	0.0345/0.0637
$R1$, w$R2$ (all data)	0.0332/0.0541	0.0274/0.0548	0.0229/0.0433	0.0408/0.0665
$\Delta\rho_{max}$ (e/Å^3)	2.24	2.95	2.11	2.72
$\Delta\rho_{min}$ (e/Å^3)	−2.83	−2.21	−1.77	−3.42

[a] $R1=\sum||F_o|-|F_c||/\sum|F_o|$, $wR2=\{\sum w[(F_o)^2-(F_c)^2]^2/\sum w[(F_o)^2]^2\}^{1/2}$.

the reciprocal lattice vector) was used to determine the number of plane waves needed for the expansion of the wave function in the interstitial region. Here, we adopted the values of 2.5, 2.5 and 2.42 au for RE, Mn and Sn atoms, respectively, as the R_{MT} radii and let $R_{MT}\times K_{MAX}=7$. In addition, we used the separate energy of −8.0 Ry between the valence and core states. Thus, the *RE*–4*f*5*d*6*s*, Mn–3*d*4*s* and Sn–5*s*5*p* orbitals were treated as valence states, while *RE*–4*d*5*s*5*p*, Mn–3*s*3*p* and Sn–4*p*4*d* orbitals were acted as semicore states, with other electrons as core states. We calculated the total energy and magnetic moments with 100, 200 300 *k*-points for both compounds, and the results suggested that the calculated results did not change much from 100 to 300 *k*-points. Therefore in this study, we used the 200 *k*-point in the complete Brillouin zone, and the Brillouin zone integration was carried out with a modified tetrahedron method [48]. Self-consistency calculation of electronic structure was achieved when the total-energy variation from iteration to iteration converged to be 0.01 mRy accuracy or better. The Fermi level was selected as the energy reference ($E_F=0$ eV). Furthermore, to improve the description of the strongly correlated 4*f* and 3*d* electrons, we also introduced the on-site Coulomb energy *U* correction, namely the GGA+*U*-type calculation [49].

3. Results and discussion

3.1. Structural descriptions

The structures of RE_3MnSn_{5-x} ($x=0.16(6)$ (**1**), 0.29(1) (**2**) for *RE*=Tm, $x=0.05(8)$ (**3**), 0.21(3) (**4**) for *RE*=Lu) belong to the $Hf_3Cr_2Si_4$ type with RE atoms filling the Hf sites, Mn and one Sn (8*d* site) atom replacing the Cr sites, and other Sn atoms corresponding to the Si sites [41]. It is found that the unit cell volume of RE_3MnSn_{5-x} (*RE*=Tm, Lu) increase with the increase in radii of rare earth ions and content of Sn element. The structures of RE_3MnSn_{5-x} feature a 3D framework composed of 1D $[Mn_2Sn_7]$ chains interconnected by $[Sn_3]$ double chains via Sn–Sn bonds forming large tunnels along the *b*-axis made by $[Mn_4Sn_{16}]$ 20-memebered rings, which are occupied by a mass of rare earth atoms (Fig. 1a). Since all compounds are isostructural, the structure of compound **1** will be discussed in detail as a representative.

The 1D $[Mn_2Sn_7]$ chain can be viewed as being formed by $[Mn_2Sn_5]$ chains and linear Sn single chains interconnected via Sn–Sn bonds. Each Mn(1) atom is surrounded by five unique Sn atoms (Sn(1), Sn(2), Sn(3), Sn(4) and Sn(5) atoms) in a severely distorted square pyramidal geometry. A short Sn(3)–Sn(5) bond of 2.924(2) Å can be found within the $[MnSn_5]$ polyhedron. Adjacent $[MnSn_5]$ polyhedra are interconnected via face- and edge-sharing to form 1D $[Mn_2Sn_5]$ chain along the *b*-axis (Fig. 2a). The Mn–Sn bond distances fall in the narrow range of 2.747(2)–2.810(2) Å for compound **1** and 2.743(1)–2.805(1) Å for compound **3**, respectively. These Mn–Sn distances are comparable to those reported in other related compounds such as $Yb_4Mn_2Sn_5$ (2.790–2.791 Å) [20], $Tm_4Mn_4Sn_7$ (2.748–2.825 Å) [39] and $TmMn_6Sn_6$ (2.754–2.861 Å) [50]. The 1D linear Sn chain is formed by Sn(6) atoms with alternating Sn(6)–Sn(6) distances of 2.976(2) and 3.086(2) Å (Fig. 3a), which is slightly different from the linear Sn chain with well-proportioned Sn–Sn distance of 2.909(8) Å in $Tm_4Mn_4Sn_7$ [39]. The $[Mn_2Sn_5]$ chain is attached by the linear Sn chain via Sn(5)–Sn(6) bonds of 2.980(1) Å to form the 1D $[Mn_2Sn_7]$ chain along the *b*-axis.

Another building unit is the $[Sn_3]$ double chains formed by Sn(7) and Sn(8) atoms. The Sn(7) atoms form a linear chain along the *b*-axis with alternating Sn(7)–Sn(7) bonds of 3.001(2) and 3.061(2) Å, which is similar to that composed of Sn(6) atoms. Two parallel Sn linear chains are bridged by Sn(8) atoms alternatively on both sides to form $[Sn_3]$ double chains along the *b*-axis (Fig. 3b). The Sn(8) atom is 0.913 Å away from the plane formed by parallel Sn chains with Sn(7)–Sn(8) distances of 3.040(1) and 3.130 (1) Å. It is well known that Sn element is capable of forming various types of 1D chains, such as linear chain in $Tm_4Mn_4Sn_7$ [39], uniform zigzag chain in $SrNiSn_2$ [51], distorted zigzag $[Sn_2]$ chains in Sm_2NiSn_4 [17] and zigzag $[Sn_3]$ chains in Yb_3CoSn_6 and another type of zigzag $[Sn_3]$ chain in $Yb_4Mn_2Sn_5$ [20]. It should be noted that the $[Sn_3]$ double chain in Tm_3MnSn_{5-x} is different from the zigzag $[Sn_3]$ single chain in $Yb_4Mn_2Sn_5$ (Fig. 3c). To the best of our knowledge, such $[Sn_3]$ double chain in Tm_3MnSn_{5-x} has not been reported yet.

Table 2
Atomic coordinates and equivalent displacement parameters ($Å^2 \times 10^3$) for the title compounds.

Atom	Wyckoff	x	y	z	U(eq)[a]
1					
Tm(1)	4c	0.3498(1)	1/4	0.3173(1)	8(1)
Tm(2)	4c	0.4428(1)	3/4	0.7384(1)	7(1)
Tm(3)	4c	0.2106(1)	1/4	0.6812(1)	7(1)
Tm(4)	4c	0.4383(1)	3/4	0.9695(1)	9(1)
Tm(5)	4c	0.4653(1)	3/4	0.3493(1)	8(1)
Tm(6)	4c	0.3237(1)	1/4	0.0308(1)	10(1)
Mn(1)	8d	0.1858(1)	0.4905(2)	0.3385(1)	9(1)
Sn(1)	4c	0.3050(1)	3/4	0.3844(1)	9(1)
Sn(2)	4c	0.2335(1)	1/4	0.4824(1)	9(1)
Sn(3)	4c	0.3781(1)	1/4	0.7045(1)	12(1)
Sn(4)	4c	0.2208(1)	1/4	0.1848(1)	9(1)
Sn(5)	4c	0.4333(1)	1/4	0.8875(1)	15(1)
Sn(6)	8d	0.4340(1)	0.4955(1)	0.1584(1)	8(1)
Sn(7)	8d	0.3673(1)	0.5025(1)	0.5400(1)	10(1)
Sn(8)	4c	0.4849(1)	1/4	0.4418(1)	10(1)
2					
Tm(1)	4c	0.3498(1)	1/4	0.3176(1)	6(1)
Tm(2)	4c	0.4424(1)	3/4	0.7376(1)	6(1)
Tm(3)	4c	0.2106(1)	1/4	0.6815(1)	5(1)
Tm(4)	4c	0.4383(1)	3/4	0.9693(1)	7(1)
Tm(5)	4c	0.4654(1)	3/4	0.3504(1)	6(1)
Tm(6)	4c	0.3243(1)	1/4	0.0300(1)	8(1)
Mn(1)	8d	0.1855(1)	0.4911(2)	0.3383(1)	8(1)
Sn(1)	4c	0.3054(1)	3/4	0.3854(1)	7(1)
Sn(2)	4c	0.2346(1)	1/4	0.4826(1)	8(1)
Sn(3)	4c	0.3781(1)	1/4	0.7034(1)	9(1)
Sn(4)	4c	0.2205(1)	1/4	0.1837(1)	8(1)
Sn(5)	4c	0.4334(1)	1/4	0.8855(1)	15(1)
Sn(6)	8d	0.4344(1)	0.4957(1)	0.1587(1)	6(1)
Sn(7)	8d	0.3677(1)	0.5033(1)	0.5397(1)	8(1)
Sn(8)	4c	0.4850(1)	1/4	0.4425(1)	8(1)
3					
Lu(1)	4c	0.3490(1)	1/4	0.3181(1)	8(1)
Lu(2)	4c	0.4438(1)	3/4	0.7392(1)	8(1)
Lu(3)	4c	0.2118(1)	1/4	0.6820(1)	8(1)
Lu(4)	4c	0.4373(1)	3/4	0.9694(1)	10(1)
Lu(5)	4c	0.4648(1)	3/4	0.3492(1)	8(1)
Lu(6)	4c	0.3217(1)	1/4	0.0326(1)	10(1)
Mn(1)	8d	0.1851(1)	0.4887(2)	0.3393(1)	10(1)
Sn(1)	4c	0.3047(1)	3/4	0.3844(1)	9(1)
Sn(2)	4c	0.2338(1)	1/4	0.4835(1)	10(1)
Sn(3)	4c	0.3794(1)	1/4	0.7060(1)	12(1)
Sn(4)	4c	0.2200(1)	1/4	0.1862(1)	10(1)
Sn(5)	4c	0.4329(1)	1/4	0.8927(1)	15(1)
Sn(6)	8d	0.4326(1)	0.4952(1)	0.1589(1)	8(1)
Sn(7)	8d	0.3676(1)	0.5025(1)	0.5409(1)	7(1)
Sn(8)	4c	0.4847(1)	1/4	0.4414(1)	10(1)
4					
Lu(1)	4c	0.3494(1)	1/4	0.3181(1)	9(1)
Lu(2)	4c	0.4429(1)	3/4	0.7383(1)	9(1)
Lu(3)	4c	0.2110(1)	1/4	0.6821(1)	8(1)
Lu(4)	4c	0.4378(1)	3/4	0.9692(1)	11(1)
Lu(5)	4c	0.4650(1)	3/4	0.3499(1)	9(1)
Lu(6)	4c	0.3234(1)	1/4	0.0311(1)	12(1)
Mn(1)	8d	0.1850(1)	0.4909(3)	0.3390(1)	10(1)
Sn(1)	4c	0.3050(1)	3/4	0.3852(1)	9(1)
Sn(2)	4c	0.2341(1)	1/4	0.4832(1)	11(1)
Sn(3)	4c	0.3786(1)	1/4	0.7044(1)	12(1)
Sn(4)	4c	0.2205(1)	1/4	0.1848(1)	10(1)
Sn(5)	4c	0.4333(1)	1/4	0.8895(1)	18(1)
Sn(6)	8d	0.4337(1)	0.4955(1)	0.1588(1)	8(1)
Sn(7)	8d	0.3677(1)	0.5031(2)	0.5401(1)	10(1)
Sn(8)	4c	0.4849(1)	1/4	0.4419(1)	11(1)

[a] U(eq) is defined as one-third of the trace of the orthogonalized U_{ij} tensor.

Table 3
The bond distances (Å) in compounds **1** and **2**.

Bond	Distance (Å)	Bond	Distance (Å)
1			
Tm(1)–Sn(4)	3.102(1)	Tm(4)–Sn(2)	3.184(2)
Tm(1)–Sn(8)	3.119(1)	Tm(4)–Sn(5)	3.197(2)
Tm(1)–Sn(6)	3.210(1) × 2	Tm(4)–Sn(6)	3.223(1) × 2
Tm(1)–Sn(2)	3.276(1)	Tm(4)–Sn(5)	3.272(1) × 2
Tm(1)–Sn(1)	3.299(1) × 2	Tm(4)–Mn(1)	3.354(2) × 2
Tm(1)–Mn(1)	3.379(2) × 2	Tm(4)–Sn(6)	3.385(1) × 2
Tm(2)–Sn(8)	3.012(1)	Tm(5)–Sn(3)	3.007(2)
Tm(2)–Sn(4)	3.132(2)	Tm(5)–Sn(1)	3.011(2)
Tm(2)–Sn(6)	3.130(1) × 2	Tm(5)–Sn(8)	3.261(2)
Tm(2)–Mn(1)	3.167(2) × 2	Tm(5)–Sn(6)	3.301(1) × 2
Tm(2)–Sn(3)	3.299(1) × 2	Tm(5)–Sn(8)	3.352(1) × 2
Tm(2)–Sn(7)	3.617(1) × 2	Tm(6)–Sn(5)	2.951(2)
Tm(3)–Sn(2)	3.008(1)	Tm(6)–Sn(4)	2.990(1)
Tm(3)–Sn(1)	3.056(1)	Tm(6)–Sn(6)	3.167(1) × 2
Tm(3)–Sn(6)	3.106(1) × 2	Tm(6)–Sn(1)	3.2360(1)
Tm(3)–Sn(3)	3.117(1)	Tm(6)–Sn(2)	3.291(1) × 2
Tm(3)–Sn(4)	3.286(1) × 2	Tm(6)–Mn(1)	C(2) × 2
Tm(3)–Mn(1)	3.420(2) × 2	Sn(3)–Sn(5)	2.924(2)
Mn(1)–Sn(2)	2.747(2)	Sn(3)–Sn(7)	2.908(1) × 2
Mn(1)–Sn(4)	2.800(2)	Sn(4)–Sn(7)	3.100(1) × 2
Mn(1)–Sn(1)	2.795(2)	Sn(5)–Sn(6)	2.980(1) × 2
Mn(1)–Sn(5)	2.804(2)	Sn(6)–Sn(6)	2.976(2)
Mn(1)–Sn(3)	2.810(2)	Sn(6)–Sn(6)	3.086(2)
Mn(1)–Mn(1)	2.915(3)	Sn(7)–Sn(7)	3.001(2)
Mn(1)–Mn(1)	3.147(3)	Sn(7)–Sn(7)	3.061(2)
Sn(1)–Sn(7)	3.001(1) × 2	Sn(7)–Sn(8)	3.040(1)
Sn(2)–Sn(7)	3.034(1) × 2	Sn(7)–Sn(8)	3.130(1)
2			
Tm(1)–Sn(4)	3.1117(9)	Tm(4)–Sn(2)	3.1962(9)
Tm(1)–Sn(8)	3.1144(9)	Tm(4)–Sn(5)	3.209(1)
Tm(1)–Sn(6)	3.2014(7) × 2	Tm(4)–Sn(6)	3.2162(7) × 2
Tm(1)–Sn(2)	3.2528(9)	Tm(4)–Sn(5)	3.2576(5) × 2
Tm(1)–Sn(1)	3.2762(4) × 2	Tm(4)–Mn(1)	3.339(1) × 2
Tm(1)–Mn(1)	3.373(1) × 2	Tm(4)–Sn(6)	3.3698(7) × 2
Tm(2)–Sn(8)	3.0050(9)	Tm(5)–Sn(3)	2.9973(9)
Tm(2)–Sn(4)	3.1113(9)	Tm(5)–Sn(1)	2.9989(9)
Tm(2)–Sn(6)	3.1218(7) × 2	Tm(5)–Sn(8)	3.2254(9)
Tm(2)–Mn(1)	3.151(1) × 2	Tm(5)–Sn(6)	3.2953(7) × 2
Tm(2)–Sn(3)	3.2724(4) × 2	Tm(5)–Sn(8)	3.3254(4) × 2
Tm(2)–Sn(7)	3.5832(8) × 2	Tm(6)–Sn(5)	2.952(1)
Tm(3)–Sn(2)	3.0036(9)	Tm(6)–Sn(4)	2.9885(9)
Tm(3)–Sn(1)	3.0590(9)	Tm(6)–Sn(6)	3.1630(7) × 2
Tm(3)–Sn(6)	3.1005(7) × 2	Tm(6)–Sn(1)	3.2222(9)
Tm(3)–Sn(3)	3.1059(9)	Tm(6)–Sn(2)	3.2740(4) × 2
Tm(3)–Sn(4)	3.2639(4) × 2	Tm(6)–Mn(1)	3.265(1) × 2
Tm(3)–Mn(1)	3.402(1) × 2	Sn(3)–Sn(5)	2.905(1)
Mn(1)–Sn(2)	2.751(1)	Sn(3)–Sn(7)	2.8868(9) × 2
Mn(1)–Sn(4)	2.800(1)	Sn(4)–Sn(7)	3.0780(9) × 2
Mn(1)–Sn(1)	2.795(1)	Sn(5)–Sn(6)	2.954(1) × 2
Mn(1)–Sn(5)	2.782(2)	Sn(6)–Sn(6)	2.9543(1)
Mn(1)–Sn(3)	2.803(1)	Sn(6)–Sn(6)	3.059(1)
Mn(1)–Mn(1)	2.899(3)	Sn(7)–Sn(7)	2.967(2)
Mn(1)–Mn(1)	3.114(3)	Sn(7)–Sn(7)	3.046(1)
Sn(1)–Sn(7)	2.9712(9) × 2	Sn(7)–Sn(8)	3.0182(9)
Sn(2)–Sn(7)	3.0124(9) × 2	Sn(7)–Sn(8)	3.1085(9)

The 1D $[Mn_2Sn_7]$ chains and $[Sn_3]$ double chains are further interconnected via Sn–Sn bonds (2.908(1)–3.100(1) Å) into a 3D $[Mn_2Sn_{10}]$ ($[MnSn_5]$) framework, forming large tunnels along the *b*-axis made by $[Mn_4Sn_{16}]$ 20-memebered rings, which are occupied by a mass of Tm atoms (Fig. 1a). Tm(1), Tm(3) and Tm(6) atoms are all surrounded by seven Sn atoms with distorted pentagonal bipyramid coordination geometries capped by two additional Mn(1) atoms, whereas Tm(5) atom has similar pentagonal bipyramidal coordination environment without capping Mn atoms. Tm(2) and Tm(4) atoms are both 10-coordinated by eight Sn atoms and two Mn atoms. The Tm–Mn and Tm–Sn distances are in the range of 3.167(2)–3.420(2) and 2.951(2)–3.617(1) Å, respectively, which are comparable with those in $Tm_4Mn_4Sn_7$ [39] and $TmMn_6Sn_6$ [50]. The Lu–Mn and Lu–Sn distances fall in the range of 3.155(1)–3.409(1)

Table 4
The bond distances (Å) in compounds **3** and **4**.

Bond	Distance (Å)	Bond	Distance (Å)
3			
Lu(1)–Sn(4)	3.0869(9)	Lu(4)–Sn(2)	3.158(1)
Lu(1)–Sn(8)	3.1042(9)	Lu(4)–Sn(5)	3.156(1)
Lu(1)–Sn(6)	3.1973(7) × 2	Lu(4)–Sn(6)	3.2235(8) × 2
Lu(1)–Sn(2)	3.2571(9)	Lu(4)–Sn(5)	3.2337(7) × 2
Lu(1)–Sn(1)	3.2840(6) × 2	Lu(4)–Mn(1)	3.309(1) × 2
Lu(1)–Mn(1)	3.361(1) × 2	Lu(4)–Sn(6)	3.4075(8) × 2
Lu(2)–Sn(8)	3.0016(9)	Lu(5)–Sn(3)	2.987(1)
Lu(2)–Sn(4)	3.119(1)	Lu(5)–Sn(1)	2.993(1)
Lu(2)–Sn(6)	3.1147(7) × 2	Lu(5)–Sn(8)	3.264(1)
Lu(2)–Mn(1)	3.155(1) × 2	Lu(5)–Sn(6)	3.2880(8) × 2
Lu(2)–Sn(3)	3.2846(6) × 2	Lu(5)–Sn(8)	3.3417(6) × 2
Lu(2)–Sn(7)	3.6024(8) × 2	Lu(6)–Sn(5)	2.927(1)
Lu(3)–Sn(2)	2.994(1)	Lu(6)–Sn(4)	2.9600(9)
Lu(3)–Sn(1)	3.040(1)	Lu(6)–Sn(6)	3.1508(7) × 2
Lu(3)–Sn(6)	3.0921(8) × 2	Lu(6)–Sn(1)	3.2128(9)
Lu(3)–Sn(3)	3.108(1)	Lu(6)–Sn(2)	3.2740(6) × 2
Lu(3)–Sn(4)	3.2736(6) × 2	Lu(6)–Mn(1)	3.295(1) × 2
Lu(3)–Mn(1)	3.409(1) × 2	Sn(3)–Sn(5)	2.958(1)
Mn(1)–Sn(2)	2.743(1)	Sn(3)–Sn(7)	2.9086(9) × 2
Mn(1)–Sn(4)	2.780(1)	Sn(4)–Sn(7)	3.0904(8) × 2
Mn(1)–Sn(1)	2.793(1)	Sn(5)–Sn(6)	3.017(1) × 2
Mn(1)–Sn(5)	2.803(1)	Sn(6)–Sn(6)	2.965(1)
Mn(1)–Sn(3)	2.805(1)	Sn(6)–Sn(6)	3.080(1)
Mn(1)–Mn(1)	2.886(2)	Sn(7)–Sn(7)	2.992(1)
Mn(1)–Mn(1)	3.158(3)	Sn(7)–Sn(7)	3.053(1)
Sn(1)–Sn(7)	3.0080(8) × 2	Sn(7)–Sn(8)	3.0322(8)
Sn(2)–Sn(7)	3.0238(9) × 2	Sn(7)–Sn(8)	3.1153(9)
4			
Lu(1)–Sn(4)	3.0923(2)	Lu(4)–Sn(2)	3.168(2)
Lu(1)–Sn(8)	3.100(2)	Lu(4)–Sn(5)	3.169(2)
Lu(1)–Sn(6)	3.195(1) × 2	Lu(4)–Sn(6)	3.211(2) × 2
Lu(1)–Sn(2)	3.247(2)	Lu(4)–Sn(5)	3.230(2) × 2
Lu(1)–Sn(1)	3.268(1) × 2	Lu(4)–Mn(1)	3.309(2) × 2
Lu(1)–Mn(1)	3.366(2) × 2	Lu(4)–Sn(6)	3.374(1) × 2
Lu(2)–Sn(8)	2.995(2)	Lu(5)–Sn(3)	2.987(2)
Lu(2)–Sn(4)	3.108(2)	Lu(5)–Sn(1)	2.988(2)
Lu(2)–Sn(6)	3.109(1) × 2	Lu(5)–Sn(8)	3.236(2)
Lu(2)–Mn(1)	3.141(2) × 2	Lu(5)–Sn(6)	3.282(2) × 2
Lu(2)–Sn(3)	3.265(2) × 2	Lu(5)–Sn(8)	3.321(2) × 2
Lu(2)–Sn(7)	3.582(2) × 2	Lu(6)–Sn(5)	2.921(2)
Lu(3)–Sn(2)	2.994(2)	Lu(6)–Sn(4)	2.970(2)
Lu(3)–Sn(1)	3.039(2)	Lu(6)–Sn(6)	3.147(1) × 2
Lu(3)–Sn(6)	3.088(2) × 2	Lu(6)–Sn(1)	3.209(2)
Lu(3)–Sn(3)	3.099(2)	Lu(6)–Sn(2)	3.262(1) × 2
Lu(3)–Sn(4)	3.255(2) × 2	Lu(6)–Mn(1)	3.261(2) × 2
Lu(3)–Mn(1)	3.397(2) × 2	Sn(3)–Sn(5)	2.935(2)
Mn(1)–Sn(2)	2.742(2)	Sn(3)–Sn(7)	2.887(2) × 2
Mn(1)–Sn(4)	2.792(2)	Sn(4)–Sn(7)	3.077(2) × 2
Mn(1)–Sn(1)	2.787(2)	Sn(5)–Sn(6)	2.971(2) × 2
Mn(1)–Sn(5)	2.777(2)	Sn(6)–Sn(6)	2.948(2)
Mn(1)–Sn(3)	2.794(2)	Sn(6)–Sn(6)	3.055(2)
Mn(1)–Mn(1)	2.892(4)	Sn(7)–Sn(7)	2.965(2)
Mn(1)–Mn(1)	3.111(4)	Sn(7)–Sn(7)	3.038(3)
Sn(1)–Sn(7)	2.976(2) × 2	Sn(7)–Sn(8)	3.015(2)
Sn(2)–Sn(7)	3.010(2) × 2	Sn(7)–Sn(8)	3.099(2)

and 2.927(1)–3.6024(8) Å, respectively, for compound **3**. In Lu_3MnSn_{5-x} phases, most of the Mn–Sn and Sn–Sn lengths are slightly shorter than those of Tm_3MnSn_{5-x} phases, which is in accordance with the radii of rare earth ions. In addition, it is found that most of the bond distances are decreased with the decrease in the Sn element, that is, the deficiency on some Sn sites slightly shorten the Mn–Sn and Sn–Sn bonds.

One prominent feature for the structure of Tm_3MnSn_{5-x} is the 1D $[Mn_2Sn_5]$ chain, in which Mn(1) atom is coordinated by five Sn atoms with a greatly distorted square pyramidal geometry and features 1D linear chain with alternant Mn–Mn bonds of 2.915(3) and 3.147(3) Å (Fig. 2a). The former is comparable with the longest Mn–Mn distances in elemental α-Mn (*I*4-3*m*; 2.895 and 2.931 Å) [52]. So far, there have been several similar 1D linear Mn chains in related ternary Tm–Mn–*Tt* (*Tt*=Si, Sn) phases, such as $Tm_4Mn_4Sn_7$ and $Tm_2Mn_3Si_5$, in which the Mn atoms are coordinated by six tetrel atoms. In $Tm_4Mn_4Sn_7$, the $[MnSn_6]$ octahedra are condensed via face-sharing to form 1D $[MnSn_3]$ chain and Mn atoms feature 1D linear chain with equal Mn–Mn bonds of 2.918(1) Å (Fig. 2b) [39]. In $Tm_2Mn_3Si_5$, the $[MnSi_6]$ polyhedra are fused via edge-sharing to form 1D $[MnSn_4]$ chain and Mn atoms feature linear chain with shorter Mn–Mn bonds of 2.692(1) Å (Fig. 2c) [40]. Similar bonding characters for Mn atoms have also been reported for many ternary manganese antimonides [53–55].

The most closely related structure to Tm_3MnSn_{5-x} in the framework feature is the $Tm_4Mn_4Sn_7$ structure. For the sake of clarity only, we describe their structures as composed of 1D $[Mn_2Sn_5]$ chain, linear Sn chain and $[Sn_3]$ double chain in Tm_3MnSn_{5-x}, whereas 1D $[MnSn_3]$ chain and linear Sn chain in $Tm_4Mn_4Sn_7$. In Tm_3MnSn_{5-x}, the 1D $[Mn_2Sn_5]$ chains are bridged by $[Sn_3]$ double chains to form 3D $[Mn_2Sn_8]$ framework with large tunnels made by $[Mn_4Sn_{16}]$ 20-memebered rings, which are transfixed by 1D Sn linear chain interconnecting to the 3D framework via Sn–Sn bonds (Fig. 1a). In $Tm_4Mn_4Sn_7$, the 1D $[MnSn_3]$ chains are directly condensed via edge-sharing and Sn–Sn bonds to form 3D $[Mn_4Sn_6]$ framework with smaller tunnels made by $[Mn_8Sn_8]$ 16-memebered rings along the *c*-axis, which are transfixed by isolate 1D Sn linear chain without direct Sn–Sn contacts to the $[Mn_4Sn_6]$ framework (Fig. 1b). All the Tm atoms encapsulated within the tunnels feature tube-like arrangements, the center of which are transfixed by linear 1D Sn chains for both compounds.

3.2. Transport properties and electronic structure

To assess the feasibility of RE_3MnSn_{5-x} as magnetic resistance materials, preliminary measurements of their charge transport properties have been made. The present measurements are on unoptimized samples and further work will be necessary to understand how the level of Sn deficiencies affects these properties. The results of resistivity measurements for two compounds are presented in Fig. 4. Both compounds show typical metallic-like behavior. Their resistivities at room temperature are of the order of 135–200 μΩ cm, and they decrease continuously upon cooling and reach 85–100 μΩ cm at 5 K. Furthermore, we also examine their resistivities at various applied magnetic fields up to 5 T. It is found that their resistivities are almost unchanged at various magnetic fields for both compounds.

To investigate the electronic properties of the title compounds, we carried out accurate band structure calculation by using the FPLAPW method. The spin polarizations were properly taken into account by considering the *f*-electron of rare earth atoms and *d*-electron of manganese atoms. The electronic calculations were performed on hypothetical "RE_3MnSn_5" modes, in which all the Sn sites were considered as fully occupied. The calculated total density of states (TDOS) and partial density of states (PDOS) from each element for "Lu_3MnSn_5" are given in Fig. 5a. It is seen that the Fermi level fall in the nonzero area with large density of states, indicating that Lu_3MnSn_5 is metallic. Below the Fermi level, the states in the energy range of −5 to 0 eV are essentially dominated by Sn 5*p* and Mn 3*d* electrons, and the states in the energy range of −10 to −5.3 eV are mainly contributed by the Sn 5*s* electrons. The narrow peaks located at about −5.0 eV below the Fermi level belong to the fully occupied Lu 4*f* states. The Mn 3*d* orbitals show the large spin splitting. The states with spin up are completely occupied while most of the states for spin down are almost empty. The PDOS of Sn atoms spread over the whole

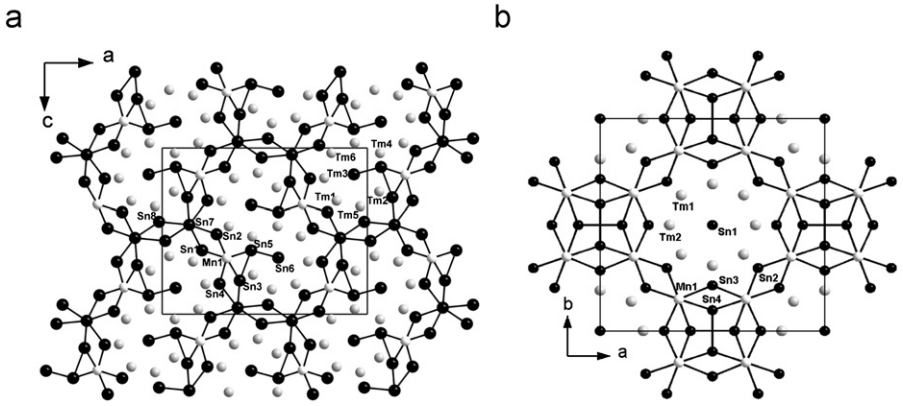

Fig. 1. View of the structures of Tm_3MnSn_{5-x} along the *b*-axis (a) and $Tm_4Mn_4Sn_7$ along the *c*-axis (b). The thulium, manganese and tin atoms are drawn as gray, white and black spheres, respectively.

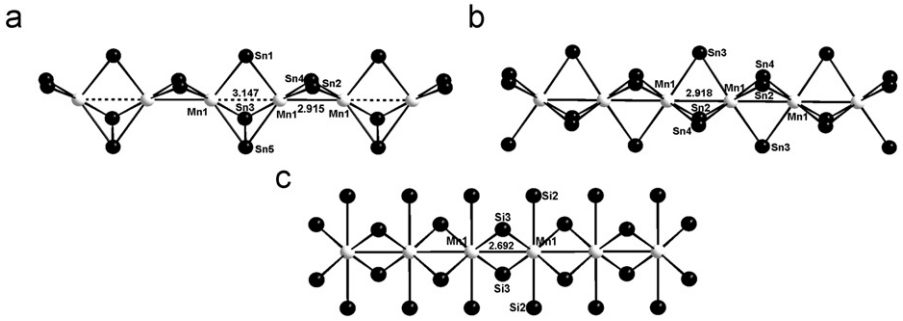

Fig. 2. Comparison of the $[Mn_2Sn_5]$ chain in Tm_3MnSn_{5-x} (a), $[MnSn_3]$ chain in $Tm_4Mn_4Sn_7$ (b) and $[MnSn_4]$ chain in $Tm_2Mn_3Si_5$ (c).

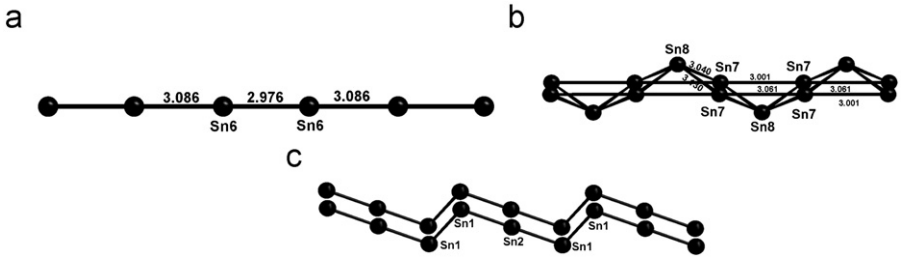

Fig. 3. View of the 1D linear chain composed of Sn(6) atoms in Tm_3MnSn_{5-x} (a), the $[Sn_3]$ double chain in Tm_3MnSn_{5-x} (b) and the zigzag $[Sn_3]$ single chain in $Yb_4Mn_2Sn_5$ (c).

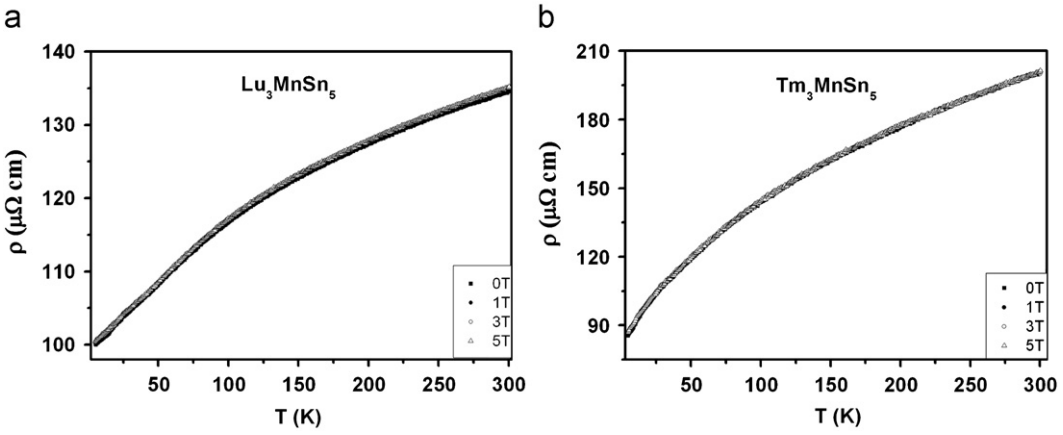

Fig. 4. Temperature dependencies of the electrical resistivities of Lu_3MnSn_5 (a) and Tm_3MnSn_5 (b) measured at various magnetic fields.

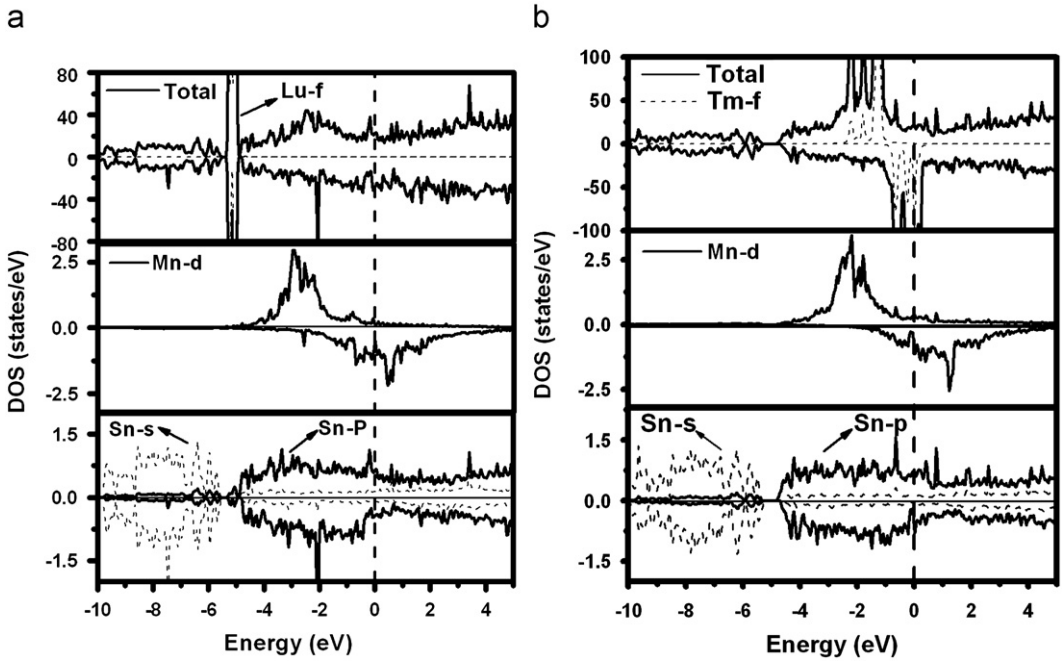

Fig. 5. Total and partial density of states (DOS) carves for hypothetical Lu_3MnSn_5 (a) and Tm_3MnSn_5 modes (b). The Fermi level is set at 0 eV.

energy range with larger dispersion, which is mostly dominated by the σ interactions between nearly free electron-like Sn 5*s*(5*p*) orbitals. It should be noted that the Sn/5*p*–Mn/3*d* mixing just below the Fermi level indicates strong covalent character of the Mn–Sn bonds. The DOS of Tm_3MnSn_5 is similar to that of Lu_3MnSn_5 except that the Tm 4*f* orbitals show small spin splitting around the Fermi level (Fig. 5b). These calculations indicate that the interactions between Sn 5*p* and Mn 3*d* orbitals around the Fermi level are mainly responsible for the metallicity of Lu_3MnSn_5 as well as the Tm 4*f* orbitals for Tm_3MnSn_5. The real structures are deficient in one or two Sn sites relative to "RE_3MnSn_5" mode, but the decrease in electron count only shift the Fermi level negligibly.

Furthermore, considering the local 3*d* and 4*f* electrons in these compounds, we further perform the GGA+*U* (on-site coulombic energy correction) type calculations to examine the correlation of *d* or *f* electrons for "Lu_3MnSn_5". It is found that the partial DOS of Lu atoms is almost unchanged except for small quantitative changes (Fig. S3). For Mn atom, the PDOS of 3*d* orbitals feature little splitting with the increase of *U* value, but there are no obvious energy shift and change. Namely, the *U* parameter does not greatly influence the energy and DOS of 3*d* and 4*f* electrons for Lu_3MnSn_5. Thus, the GGA exchange correlation formation can give sufficient and reliable results.

In summary, we have successfully obtained one type of new rare earth manganese stannides, RE_3MnSn_{5-x} (*RE*=Tm, Lu). Their structures belong to the $Hf_3Cr_2Si_4$ type and feature a 3D framework composed of 1D $[Mn_2Sn_7]$ chain interconnected by $[Sn_3]$ double chain via Sn – Sn bonds, forming 1D large tunnel along the *b*-axis occupied by the rare earth atoms. The title compounds are metallic based on electronic structure calculations as well as resistivity measurements.

Supplementary materials

X-ray crystallographic files in CIF format for the title compounds, tables of anisotropic displacement parameters, figures of the coordination geometries around the rare earth atoms, calculated DOS based on GGA+*U* type calculation, and simulated and experimental XRD powder patterns for two compounds.

Acknowledgments

We thank the financial supports from the National Nature Science Foundation of China (Nos. 20573113, 20825104, 20731006 and 20821061).

Appendix A. Supporting information

Supplementary data associated with this article can be found in the online version at doi:10.1016/j.jssc.2010.07.003.

References

[1] J.R. Salvador, C. Malliakas, J.R. Gour, M.G. Kanatzidis, Chem. Mater. 17 (2005) 1636.
[2] M.-K. Han, Y.-Q. Wu, M. Kramer, B. Vatovez, F. Grandjean, G.J. Long, G.J. Miller, Inorg. Chem. 45 (2006) 10503.
[3] J.R. Salvador, J.R. Gour, D. Bilc, S.D. Mahanti, M.G. Kanatzidis, Inorg. Chem. 43 (2004) 1403.
[4] H. Bie, O.Y. Zelinska, A.V. Tkachuk, A. Mar, Chem. Mater. 19 (2007) 4613.
[5] J.R. Salvador, D. Bilc, J.R. Gour, S.D. Mahanti, M.G. Kanatzidis, Inorg. Chem. 44 (2005) 8670.
[6] R. Pöttgen, Z. Naturforsch. 61b (2006) 677.
[7] M.G. Kanatzidis, R. Pöttgen, W. Jeitschko, Angew. Chem. Int. Ed. 44 (2005) 6996.
[8] R.V. Skolozdra, in: K.A. Gschneidner Jr., L. Eyring (Eds.), Handbook on the Physics and Chemistry of Rare Earths, 24, Elsvier, Amsterdam1997, p. 164.
[9] R. Pöttgen, R.-D. Hoffmann, R. Müllmann, B.D. Mosel, G. Kotzyba, Chem. Eur. J. 3 (1997) 1852.
[10] C.P. Sebastian, L. Zhang, C. Fehse, R.-D. Hoffmann, H. Eckert, R. Pöttgen, Inorg. Chem. 46 (2007) 771.
[11] R.-D. Hoffmann, R. Pöttgen, D. Kussmann, R. Müllmann, B.D. Mosel, Chem. Mater. 13 (2001) 4019.
[12] J.L. Hodeau, J. Chenavas, M. Marezio, J.P. Remeika, Solid State Commun. 36 (1980) 839.
[13] N.G. Patil, S. Ramakrishnan, Phys. Rev. B 59 (1999) 9581.
[14] D. Niepmann, R. Pöttgen, B. Künnen, G. Kotzyba, C. Rosenhahn, B.D. Mosel, Chem. Mater. 11 (1999) 1597.

[15] D. Niepmann, R. Pöttgen, B. Künnen, G. Kotzyba, B.D. Mosel, Chem. Mater. 12 (2000) 533.
[16] M.L. Fornasini, P. Manfrinetti, D. Mazzone, P. Riani, G. Zanicchi, J. Solid State Chem. 177 (2004) 1919.
[17] Z.-M. Sun, D.-C. Pan, X.-W. Lei, J.-G. Mao., J. Solid State Chem. 179 (2006) 3378.
[18] M.A. Zhuravleva, D. Bilc, S.D. Mahanti, M.G. Kanatzidis, Z. Anorg. Allg. Chem. 629 (2003) 327.
[19] E.L. Thomas, H.-O. Lee, A.N. Bankston, S. MaQuilon, P. Klavins, M. Moldovan, D.P. Young, Z. Fisk, J.Y. Chan, J. Solid State Chem. 179 (2006) 1641.
[20] X.-W. Lei, G.-H. Zhong, M.-J. Li, J.-G. Mao, J. Solid State Chem. 181 (2008) 2448.
[21] G.-H. Zhong, X.-W. Lei, J.-G. Mao, Phys. Rev. B. 79 (2009) 094424.
[22] X.-W. Lei, G.-H. Zhong, C.-L. Hu, J.-G. Mao, J. Alloys Compd. 485 (2009) 124.
[23] R. Pöttgen, P.E. Arpe, C. Felser, D. Kußmann, R. Müllmann, B.D. Mosel, B. Künnen, G. Kotzyba, J. Solid State Chem. 145 (1999) 668.
[24] E.K. Okudzeto, E.L. Thomas, M. Moldovan, D.P. Young, J.Y. Chan, Physica B 403 (2008) 1628.
[25] B. Chevalier, J. Etourneau, J. Mater. Chem. 9 (1999) 1789.
[26] D. Kaczorowski, K. Gofryk, L. Romaka, Ya. Mudryk, M. Monyk, P. Rogl, Intermetallics 13 (2005) 484.
[27] R. Welter, G. Venturini, B. Malaman, J. Alloys Compd. 206 (1994) 55.
[28] R. Welter, G. Venturini, E. Ressouche, B. Malaman, J. Alloys Compd. 228 (1995) 59.
[29] D. Rossi, R. Marazza, D. Mazzone, R. Ferro, J. Less-Common Met. 59 (1978) 79.
[30] M. Hofmann, S.J. Campbell, A. Szytula, J. Alloys Compd. 311 (2000) 137.
[31] R.B. van Dover, E.M. Gyorgy, R.J. Cava, J.J. Krajewski, R.J. Felder, W.F. Peck, Phys. Rev. B. 47 (1993) 6134.
[32] N.M. Norlidah, G. Venturini, B. Malaman, J. Alloys Compd. 268 (1998) 193.
[33] S.-H. Kim, D.-K. Seo, R.K. Kremer, J. Köhler, A. Villesuzanne, M.-H. Whangbo, Chem. Mater. 17 (2005) 6338.
[34] P. Schobinger-Papamantellos, J.H.V.J. Brabers, F.R. de Boer, K.H.J. Buschow, J. Alloys Compd. 203 (1994) 23.
[35] G.-H. Guo, H.-B. Zhang, J. Alloys Compd. 429 (2007) 46.
[36] A. Mar, C. Lefèvre, G. Venturini, J. Magn. Magn. Mater. 269 (2004) 380.
[37] P.M. Levy, S.-F. Zhang, A. Fert, Phys. Rev. Lett. 65 (1990) 1643.
[38] G. Venturini, B. Malaman, J. Alloys Compd. 261 (1997) 19.
[39] B. Malaman, G. Venturini, B. Roques, Mater. Res. Bull. 24 (1989) 231.
[40] R. Nirmala, V. Sankaranarayanan, K. Sethupathi, A.V. Morozkin, J. Alloys Compd. 325 (2001) 37.
[41] V.Ya. Markiv, N.N. Belyavina, Dop. Akad. Nauk Ukr. RSR. B, Geol. Khim. Biol. 4 (1986) 44.
[42] CrystalClear version 1. 3. 5; Rigaku Corp.: Woodlands, TX, 1999.
[43] G.M. Sheldrick, SHELX-97, Program for Crystal Structure Determination, 1997.
[44] G.K.H. Madsen, P. Blaha, K. Schwarz, E. Sjöstedt, L. Nordström, Phys. Rev. B. 64 (2001) 195134.
[45] K. Schwarz, P. Blaha, G.K.H. Madsen, Comput. Phys. Commun. 147 (2002) 71.
[46] J.P. Perdew, K. Burke, M. Ernzerhof, Phys. Rev. Lett. 77 (1996) 3865.
[47] P. Blaha, K. Schwarz, G.K.H. Madsen, D. Kvasnicka, J. Luitz, in: K. Schwarz (Ed.), WIEN2k, An Augmented Plane Wave+Local Orbitals Program for Calculating Crystal Properties, Technische Universität Wien, Austria, 2001.
[48] P.E. Blöchl, O. Jepsen, O.K. Andersen, Phys. Rev. B. 49 (1994) 16223.
[49] V.I. Anisimov, J. Zaanen, O.K. Andersen, Phys. Rev. B. 44 (1991) 943.
[50] C. Lefèvre, G. Venturini, B. Malaman, J. Alloys Compd. 354 (2003) 47.
[51] V. Hlukhyy, S. Eck, T.F. Fässler, Inorg. Chem. 45 (2006) 7408.
[52] P. Villars, L.D. Calvert (Eds.), Pearson's Handbook of Crystallographic Data for Intermetallic Phases, ASM International, Materials Park, OH, 1991.
[53] S. Bobev, J. Merz, Inorg. Chem. 45 (2006) 4047.
[54] A.P. Holm, M.M. Olmstead, S.M. Kauzlarich, Inorg. Chem. 42 (2003) 1973.
[55] S.-Q. Xia, S. Bobev, Inorg. Chem. 46 (2007) 874.